JOURNAL OF MATERIALS SCIENCE 18 (1983) 2563–2571

Transformation structures and strengthening mechanisms of laser processed Fe–Cr alloys

P. A. MOLIAN*, W. E. WOOD
Department of Materials Science and Engineering, Oregon Graduate Center, Beaverton, Oregon 97006, USA

The microstructures and microhardness of laser processed Fe–Cr surface alloys were investigated as functions of composition (5 to 50 wt % Cr) and melt penetration depth (100 to 1500 μm). The transformation structures were characterized by optical metallography and thin foil transmission electron microscopy. The microstructures were ferritic irrespective of compositions and melt depths. The alloys containing chromium up to 12 % (within the γ-phase field) exhibited a massive ferritic morphology while the alloys containing chromium more than 12% (beyond the γ-phase field) showed an equiaxed ferritic morphology. Transmission electron microscopy studies revealed that the substructure of ferrite consisted of dislocations, the dislocation density increased with increased chromium content. Melt depth, unlike composition, did not have a significant effect on the morphology and substructure of ferrite grains. Small amounts of ϵ-carbide and M_3C carbide phases were observed in these alloys. Both the carbides were found to decrease with an increase in the chromium of the fusion zone. Microhardness measurements indicated that there was an increase in hardness with an increase in the chromium content of the alloy.

1. Introduction

In recent years, the microstructures formed in binary iron alloys such as Fe–Cr, Fe–Ni, Fe–Mn and Fe–Co, on rapid quenching [1–5] stimulated efforts towards understanding the relevant mechanisms of phase transformation and associated strengthening. However the factors that control the structures obtained by rapid quenching were not completely elucidated and consistent. Several investigations of the transformations of Fe–Cr alloys were reported [1–4, 6]. These results disagreed in many important aspects particularly on the transformation of austenite to martensite in the alloys containing 0 to 10 wt % Cr. In addition to the kinetics of austenite to martensite or ferrite transformation, the morphology of transformation structures in Fe–Cr alloys received little attention and few thin foil electron microscopic observations were reported [1, 6]. The current study of Fe–Cr alloys, produced through laser surface alloying process, was directed to determine the transformation structures as functions of composition (5 to 50% Cr) and melt depth (100 to 1500 μm). The contributions to strengthening were also investigated from the microstructure and solid solution effects.

2. Experimental procedure

Low carbon iron (C < 0.01%, Si < 0.01%, Mn < 0.01%, S=0.003%, P=0.008%, received in the form of cold rolled ingot, was vacuum degassed (10^{-7} torr) at 650° C and cut to specimens of size 75 mm × 25 mm × 6.4 mm. Chromium was then

TABLE I

Laser power	900–1200 watts
Beam size	0.0066–0.040 cm
Scan rate	0.42–8.47 cm sec^{-1}
Lens	6.25 cm focal length (ZnSe)

*Presently with the Department of Mechanical Engineering, Iowa State University, Ames, IA 50011, USA.

0022–2461/83 $03.00 + .12

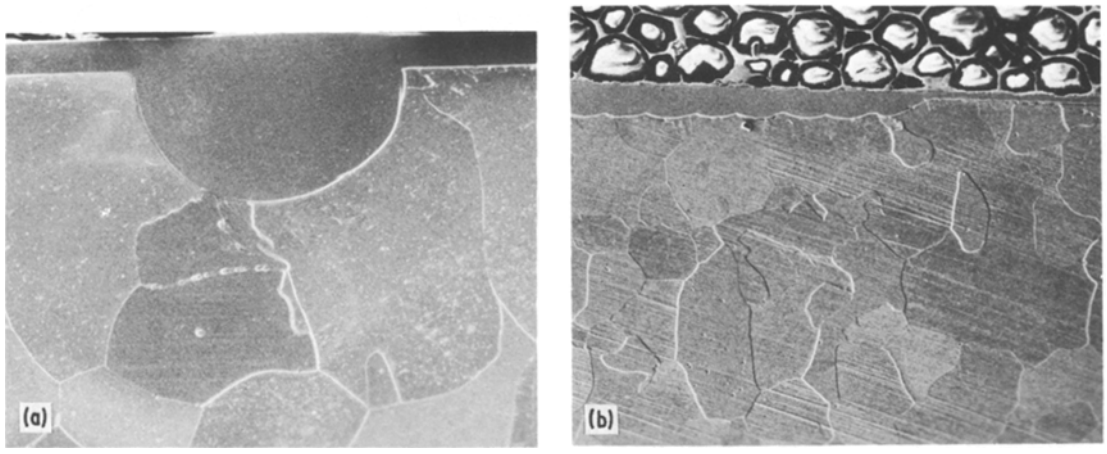

Figure 1 Scanning electron micrographs of the transverse sections of laser alloyed fusion zones showing the initial chromium coating, the fusion zone and the base iron. (a) "Single" pass; magnification: × 235. (b) "Multiple" pass; magnification: × 47.

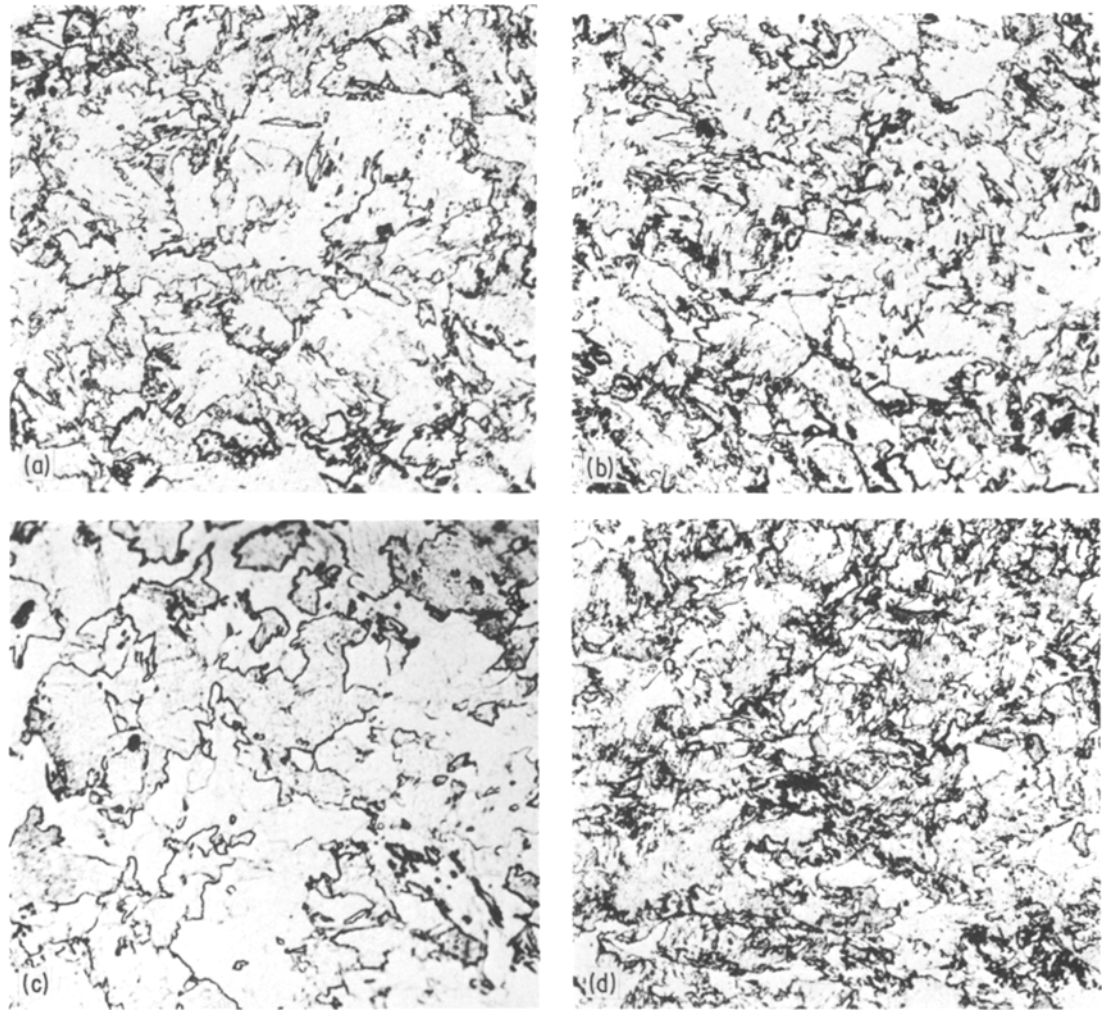

Figure 2 Optical micrographs of laser processed Fe–Cr alloys showing the massive ferrite structures. (a) 5% Cr (b) 7% Cr (c) 10% Cr alloys with a constant melt depth of 450 μm (d) 5% Cr with a shallow melt depth of 230 μm. Magnification: × 320.

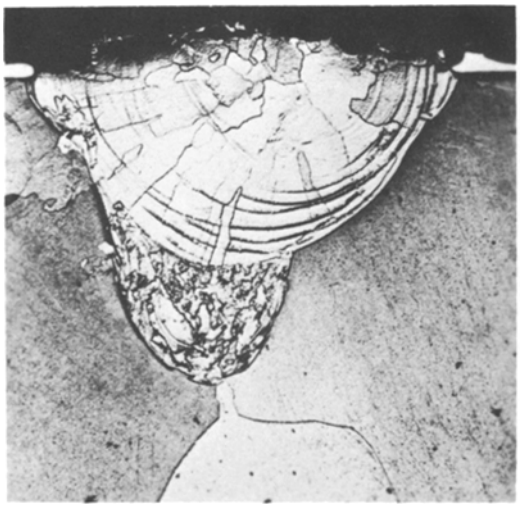

Figure 3 Optical micrograph of the fusion zone showing both "massive" and "equiaxed" ferrite structures depending on the chromium content. Magnification: × 128.

electrodeposited on these specimens using conventional plating methods. Initial chromium coatings ranged from 10 to 200 μm in thickness. After chromium deposition, the samples were again vacuum degassed at 205° C to eliminate the entrapped hydrogen in the coating.

The chromium deposited iron specimens were mounted on a numerically controlled $X-Y$ table and irradiated with a continuous wave CO_2 laser. Different laser parameters were used (Table I) to obtain melt penetration depths from 100 to 1500 μm. Both single and multiple laser passes were employed.

Microstructural and compositional analysis consisted of optical, scanning and transmission electron microscopy, and energy and wavelength dispersive X-ray microprobes. Thin foils for transmission electron microscopy were prepared according to the standard procedure and examined in a Hitachi HU-11B electron microscope operated at 100 kV. For optical and scanning electron microscopy, the samples were polished and etched in 2% nital, Villella's and mixed acid etchants. The fusion zone microhardness was determined using a Leitz miniload hardness tester.

Two heat transfer models [7, 8] were employed to study the temperature distributions and cooling rates in the fusion zones. Based on these models, the calculated cooling rates ranged from 10^3 to 10^6 ° C sec^{-1} and inversely related to the melt depths.

3. Results and discussion

3.1. Laser alloyed fusion zone studies

Fig. 1 shows the transverse sections of laser alloyed zones typically observed in single and multiple pass laser treated samples. The fusion zone studies also reveal that the desired alloy composition and cooling rate can be obtained by controlling the initial chromium coating thickness and the melt depth. For melt depths 100 to 1500 μm, the average cooling rates are estimated to be between 10^3 and 10^6 ° C sec^{-1}.

3.2. Optical metallography

3.2.1. Transformation structures of alloys within the γ-phase field

Figs. 2a to c present the optical micrographs of 5,7 and 10% Cr alloys produced to a melt depth of 450 μm (cooling rate ~ 10^4 ° C sec^{-1}) while Fig. 2d shows the microstructure of 5% Cr alloy produced to a shallow melt depth of 230 μm (cooling rate ~ 10^5 ° C sec^{-1}). A comparison of Figs. 2a through to d shows that there is no apparent change in the morphology of ferrite grains with an increase in the chromium content or the melt depth except for a change in the ferrite grain size with a decrease in melt depth. The morphology of ferrite grains being irregular in shape illustrated no apparent features that would suggest that they had arisen from a shear transformation. This type of transformation was termed as massive and was first recognized in Cu–Ga and other copper base alloys [9].

Transformation by massive mechanism was reported to occur in rapidly cooled (5.5×10^3 ° C sec^{-1}), solid-state quenched Fe–Cr (0 to 10% Cr), Fe–Ni (0 to 15% Ni) and Fe–Si (0 to 2.7% Si) alloys by Gilbert and Owen [2]. By applying Kaufmann and Cohen's thermodynamic data of regular solution analysis, they had shown that the free energy change accompanying the massive transformation (10 to 80 cal mol^{-1}) was smaller than that of the martensitic transformation (260 to 320 cal mol^{-1}) in these alloy systems. Hence they concluded that rapidly quenched Fe–Cr alloys can undergo only massive transformations. Pascover and Radcliffe [1] reported equiaxed ferrite (also designated as "massive" by them) transformations in solid-state quenched Fe–Cr alloys (0 to 10% Cr) up to quench rates of 4×10^4 ° C sec^{-1}. They also observed [10] that the structures of Fe–Cr alloys remained as equiaxed ferrite by quenching at a pressure of

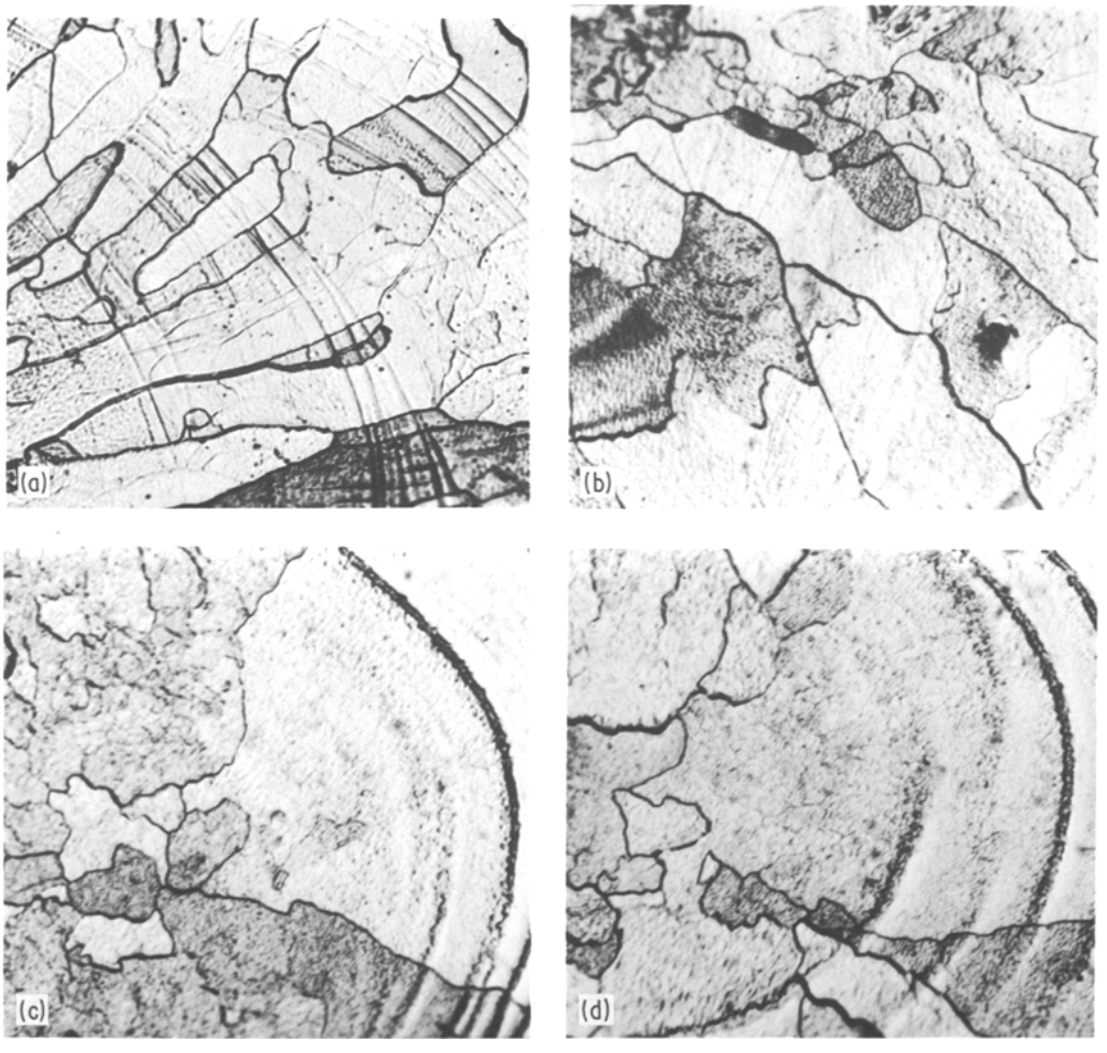

Figure 4 Optical micrographs of laser processed Fe–Cr alloys showing the equiaxed ferrite structures. (a) 20% Cr, (b) 25% Cr, (c) 30% Cr, and (d) 50% Cr. Magnification: × 320.

25 kbar (quench rate 10^2 °C sec^{-1}). They attributed that both pressure and quench rates were insufficient to inhibit the short range diffusion involved in the formation of ferrite. However Wallbridge and Parr [3] had shown the martensitic transformation in solid state quenched Fe–Cr alloys (0 to 10% Cr) with a quench rate of 1.5×10^4 °C sec^{-1} based on surface rumbling criterion. Bee and Honeycombe [6] also observed the martensitic transformation in water quenched Fe–10% Cr alloy. In fact Pascover and Radcliffe [1] reported the martensitic transformations in Fe–Cr alloys with quench rates greater than 7×10^3 °C sec^{-1} but at an alternate and lower transformation temperature of about 500° C.

Transformation temperature, i.e. the temperature at which austenite transforms to martensite or massive ferrite, plays an important role in determining the type of transformation as massive, equiaxed or martensitic. While it is well established that the transformation temperature exhibited a progressive decrease with the increase in cooling rate to a constant value in iron binary alloys, there is a discrepancy in the reported values of transformation temperature for a constant cooling rate by several investigators [1–3, 6]. Pascover and Radcliffe [1] had shown that, regardless of quench rates, martensitic transformation was observed in Fe–10% Cr alloy when the transformation temperature was around 500° C and equiaxed ferrite transformation prevailed when the transformation temperature was around

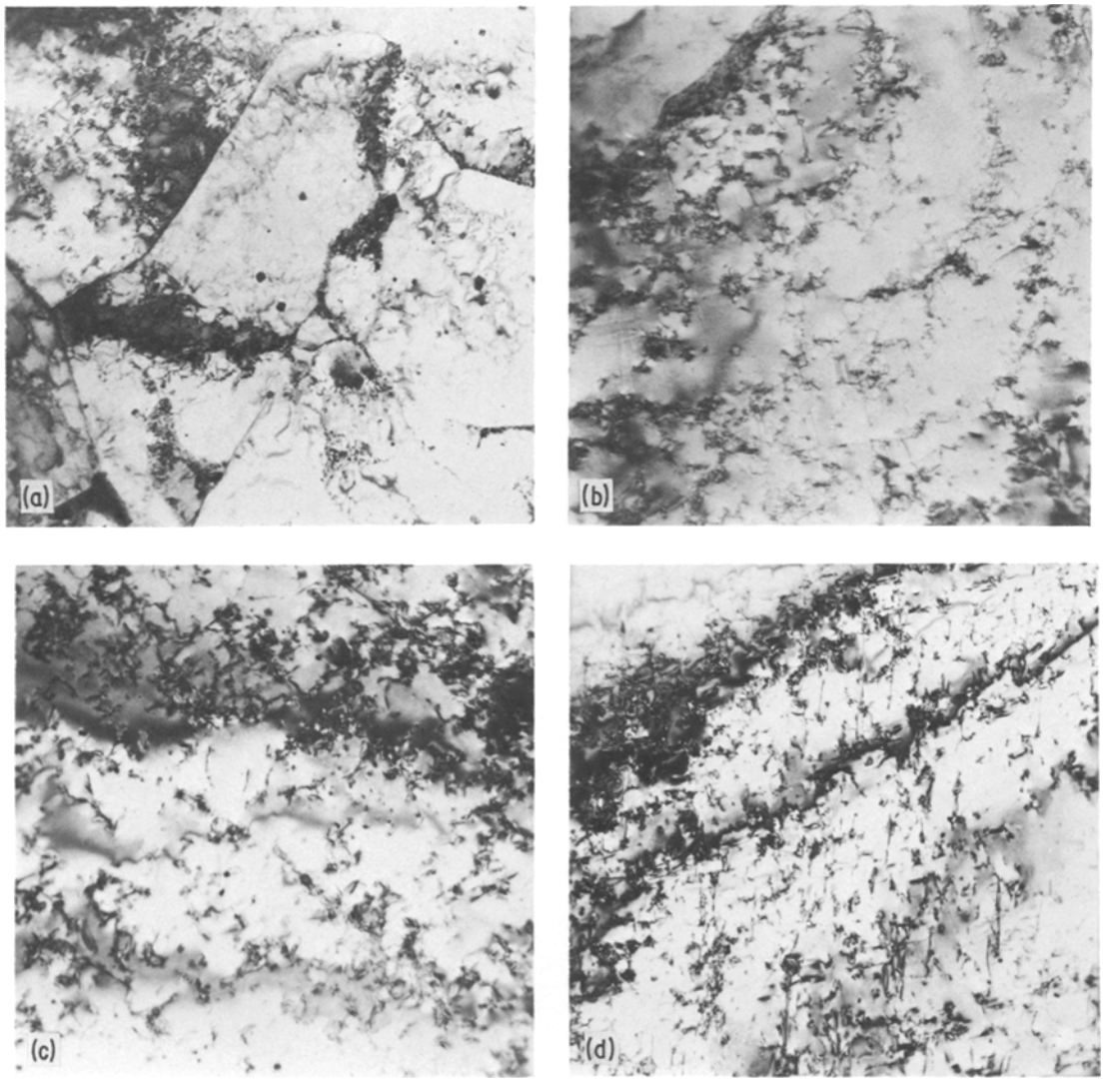

Figure 5 Transmission electron micrographs of laser processed Fe–Cr alloys showing the ferritic structures. (a) 5% Cr, (b) 10% Cr, (c) 20% Cr, and (d) 50% Cr. Magnification: × 15840.

600° C. Bee and Honeycombe [6] reported the transformation temperatures of martensite and massive to be 500 and 580° C, respectively, for Fe–10% Cr alloy. Although the transformation temperatures could not be determined in the present study, the observed characteristics of transformation behaviour in laser processed Fe–Cr alloys suggest that the transformation temperature is higher than necessary to produce the martensitic transformation. Unfortunately, there are no published data on the rapid solidification of Fe–Cr alloys with which the present results can be compared.

3.2.2. Transformation structures of alloys beyond γ-phase field

In contrast to massive ferrite structures that developed in low chromium alloys, metallographic examination of laser processed high chromium alloys revealed equiaxed ferrite structures. These ferrite grains contained several subgrains oriented in the direction of heat flow. Solute dumping lines were also evident. Figs. 3 and 4 illustrate these aspects of ferritic morphology. It is interesting to note in Fig. 3 that the microstructures vary from massive to equiaxed ferrite in the same fusion zone subject to the chromium content.

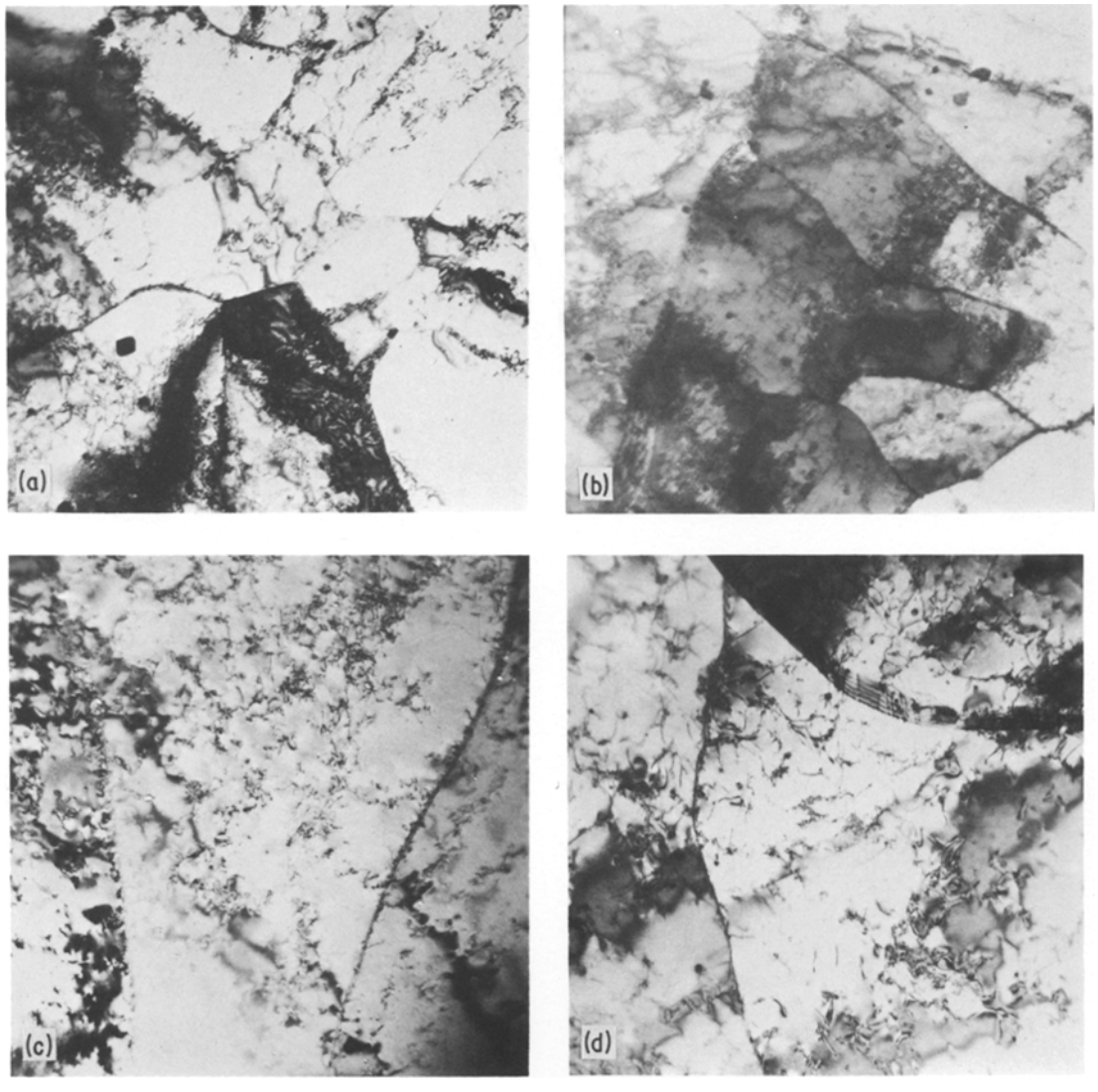

Figure 6 Transmission electron micrographs of laser processed Fe–Cr alloys showing the effect of melt depth on the microstructures. (a) 5% Cr (melt depth: 450 μm), (b) 5% Cr (melt depth: 120 μm), (c) 20% Cr (melt depth: 440 μm), (d) 20% Cr (melt depth: 100 μm). Magnification: × 15840.

3.3. Transmission electron microscopy

3.3.1. Effect of composition

Transmission electron microscopy studies revealed that all the laser processed Fe–Cr alloys were ferritic in nature, the substructure of which consisted of dislocations. For a given melt depth, an increase in dislocation density was observed qualitatively with an increase in the chromium content. Figs. 5a to d are the bright field micrographs obtained in 5, 10, 20 and 50% Cr alloys illustrating this aspect. It appears that an increase in the chromium content of the alloy caused an increase in the thermal and compositional gradients, thereby enhancing the dislocation density.

3.3.2. Effect of melt depth

Figs. 6a to d illustrate that increasing melt depths from 100 to 450 μm (decreasing the cooling rates from 10^6 to 10^4 °C sec^{-1}) did not produce a significant effect on the dislocation structures in Fe–5% Cr and Fe–20% Cr alloys. Wilson *et al.* [11] reported that there was no appreciable increase in dislocation density when the cooling rate was increased from 2×10^2 to 5×10^4 °C sec^{-1} for a Fe–5% Ni alloy.

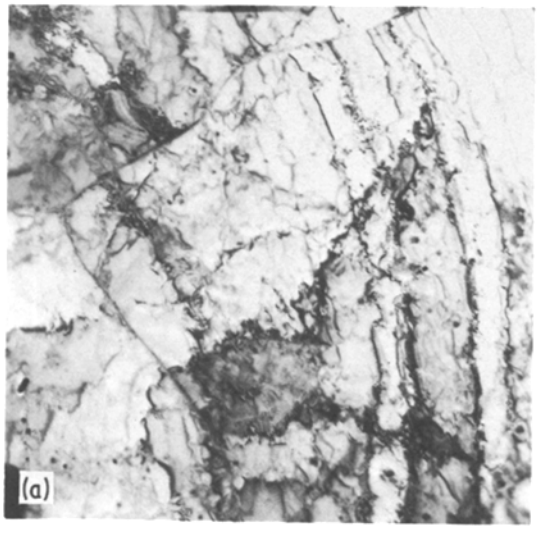

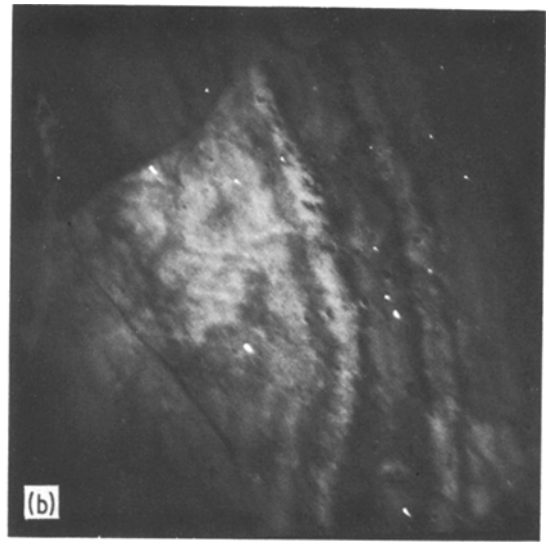

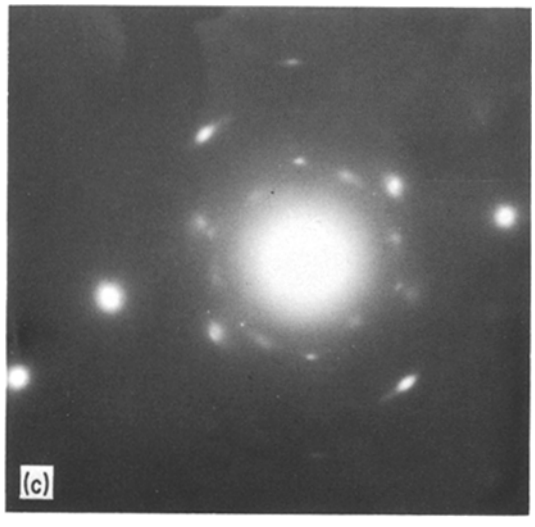

Figure 7 TEM micrographs of laser processed Fe–10% Cr alloy: (a) bright field, (b) dark field showing ϵ-carbide, and (c) SAD pattern. Magnification: × 15840.

3.3.3. Carbide precipitation

Small amounts of M_3C and ϵ-carbide phases were observed in laser processed Fe–Cr alloys and are shown in Figs. 7 to 9. Both carbides decreased with increased chromium content of the alloy. This is attributed to the effect of chromium in reducing the diffusivity of carbon and, thereby, keeping it in solution. Generally low carbon steels are not expected to contain any ϵ-carbide [12] and a minimum of 0.25% C is necessary for the precipitation of ϵ-carbide [13]. This is contrary to Tekin's results [14] who obtained ϵ-carbide in quenched 0.1% C steels. Further, the presence of ϵ-carbide in aged low carbon (C=0.01%) irons indicates that the ϵ-carbide forms in iron containing less than 0.25% C [15, 16]. ϵ-carbide was also shown to be preferentially precipitated in low carbon irons [17].

4. Microhardness

Conducted on the fusion zones, using a load of 100 g, Knoop microhardness test results as functions of composition and melt depth are shown in Fig. 10. It is apparent that an increase in hardness was obtained with an increase in the composition but not with the cooling rate. These results were consistent with the observed dislocation structures in laser processed Fe–Cr alloys. High hardness in high chromium alloys is also attributed to substitutional solid solution hardening effects.

5. Conclusions

1. The microstructures of laser processed Fe–Cr alloys were ferritic irrespective of the composition and the cooling rate.

2. The alloys containing chromium up to 12% underwent a massive transformation while the alloys containing chromium greater than 12% underwent an equiaxed ferrite transformation.

Acknowledgements

This work was partially supported by the US Army Research Office.

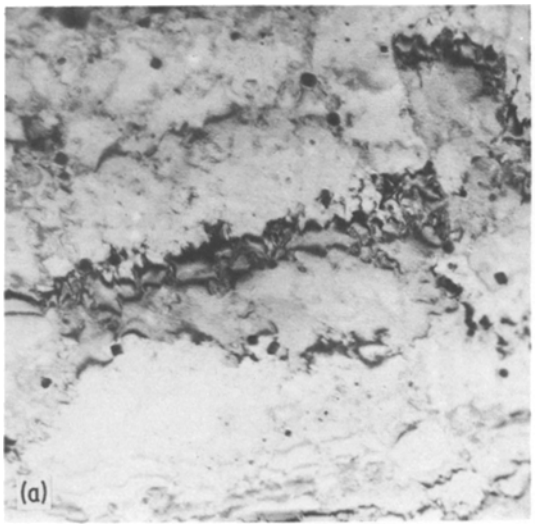

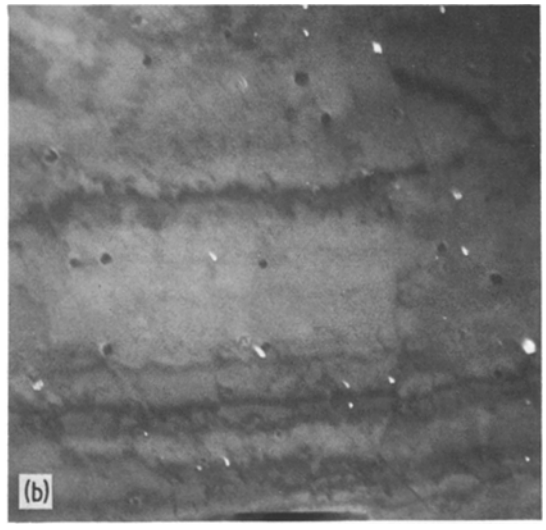

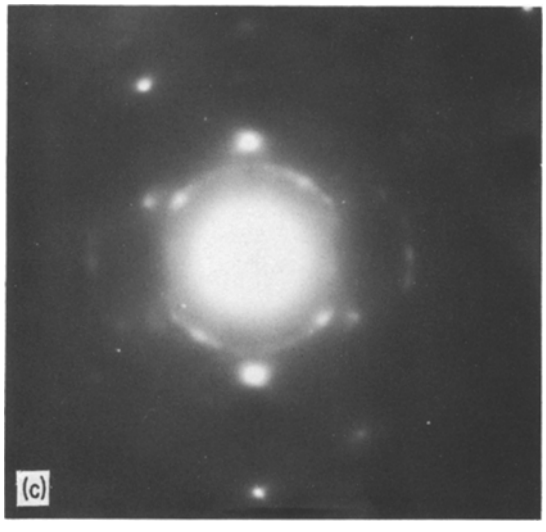

Figure 8 TEM micrographs of laser processed Fe–10% Cr alloy: (a) bright field (b) dark field showing M_3C carbide (c) SAD pattern. Magnification: × 15840.

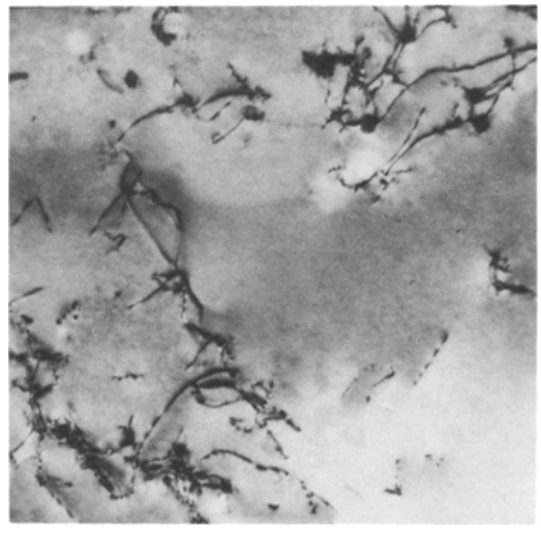

Figure 9 TEM micrograph of laser processed Fe–20% Cr alloy showing the carbide preferentially precipitated at the dislocations. Magnification: × 44000.

References

1. J. S. PASCOVER and S. V. RADCLIFFE, *Trans. AIME* **242** (1968) 673.
2. A. GILBERT and W. S. OWEN, *Acta. Met.* **10** (1962) 45.
3. J. M. WALLBRIDGE and J. G. PARR, *JISI* **204** (1966) 119.
4. M. J. BIBBY and J. G. PARR, *ibid.* **202** (1964) 100.
5. W. D. SWANSON and J. G. PARR, *ibid.* **202** (1964) 104.
6. J. V. BEE and R. W. K. HONEYCOMBE, *Met. Trans.* **9A** (1978) 587.
7. H. E. CLINE and T. R. ANTHONY, *J. Appl. Phys.* **48** (1977) 3895.
8. L. E. GREENWALD, E. M. BREINAN and B. H. KEAR, "Laser–Solid Interactions and Laser Processing" edited by S. D. Ferris (American Institute of Physics, New York, 1979) p. 189.

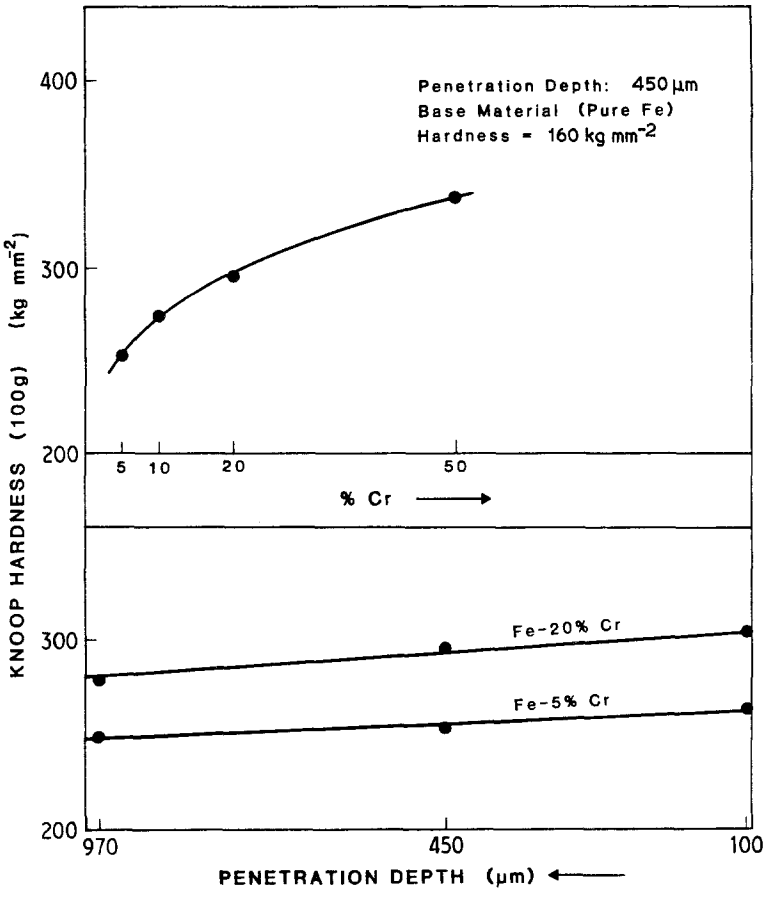

Figure 10 Effect of composition and melt penetration depth on the microhardness of laser processed Fe–Cr alloys.

9. T. B. MASSALSKI, *Acta Met.* 6 (1958) 243.
10. J. S. PASCOVER and S. V. RADCLIFFE, *Acta Met.* 17 (1969) 321.
11. T. L. WILSON, J. K. JACKSON and R. E. MINER, *Trans. AIME* 245 (1969) 2185.
12. C. S. ROBERTS, B. L. AVERBACH and M. COHEN, *Trans. ASM* 45 (1953) 576.
13. R. H. ABORN, *ibid.* 48 (1956) 51.
14. A. R. COX, *Iron and Steel* (1968) 539.
15. W. C. LESLIE, *Acta. Met.* 9 (1961) 1004.
16. M. G. H. WELLS and J. F. BUTLER, *Trans. ASM* 59 (1966) 427.
17. K. F. HALE and M. McLEAN, *JISI* 201 (1963) 331.

Received 2 August
and accepted 13 September 1982